Journal Pre-proof

Gallic acid-functionalized silver nanoparticles as colorimetric and spectrophotometric probe for detection of Al^{3+} in aqueous medium

Gajanan Ghodake, Surendra Shinde, Avinash Kadam, Rijuta Ganesh Saratale, Ganesh Dattatraya Saratale, Asad Syed, Omar Shair, Marzouq Alsaedi, Dae-Young Kim

PII: S1226-086X(19)30556-8

DOI: https://doi.org/10.1016/j.jiec.2019.10.019

Reference: JIEC 4825

To appear in: *Journal of Industrial and Engineering Chemistry*

Received Date: 22 August 2018

Revised Date: 22 July 2019

Accepted Date: 16 October 2019

Please cite this article as: Ghodake G, Shinde S, Kadam A, Saratale RG, Saratale GD, Syed A, Shair O, Alsaedi M, Kim D-Young, Gallic acid-functionalized silver nanoparticles as colorimetric and spectrophotometric probe for detection of Al^{3+} in aqueous medium, *Journal of Industrial and Engineering Chemistry* (2019), doi: https://doi.org/10.1016/j.jiec.2019.10.019

Gallic acid-functionalized silver nanoparticles as colorimetric and spectrophotometric probe for detection of Al^{3+} in aqueous medium

Gajanan Ghodake[1], Surendra Shinde[1], Avinash Kadam[2], Rijuta Ganesh Saratale[2], Ganesh Dattatraya Saratale[3], Asad Syed[4], Omar Shair[4], Marzouq Alsaedi[4], and Dae-Young Kim[1*]

[1] Department Biological and Environmental Science, College of Life Science and Biotechnology, Dongguk University-Seoul, Ilsandong-gu, 10326, Goyang-si, Gyeonggi-do, Republic of Korea

[2] Research Institute of Biotechnology and Medical Converged Science, Dongguk University-Seoul, Ilsandong-gu, Goyang-si, Gyeonggi-do, 10326, Republic of Korea

[3] Department of Food Science and Biotechnology, Dongguk University-Seoul, Ilsandong-gu, Goyang-si, Gyeonggi-do, 10326, Republic of Korea

[4] Department of Botany and Microbiology, College of Science, King Saud University, P.O. 2455, Riyadh 11451, Saudi Arabia

Corresponding author:

Dae-Young Kim, PhD

Tel: +82-31-961-5122

Fax: +82-31-961-5122

Email: sbpkim@dongguk.edu

Graphical abstract:

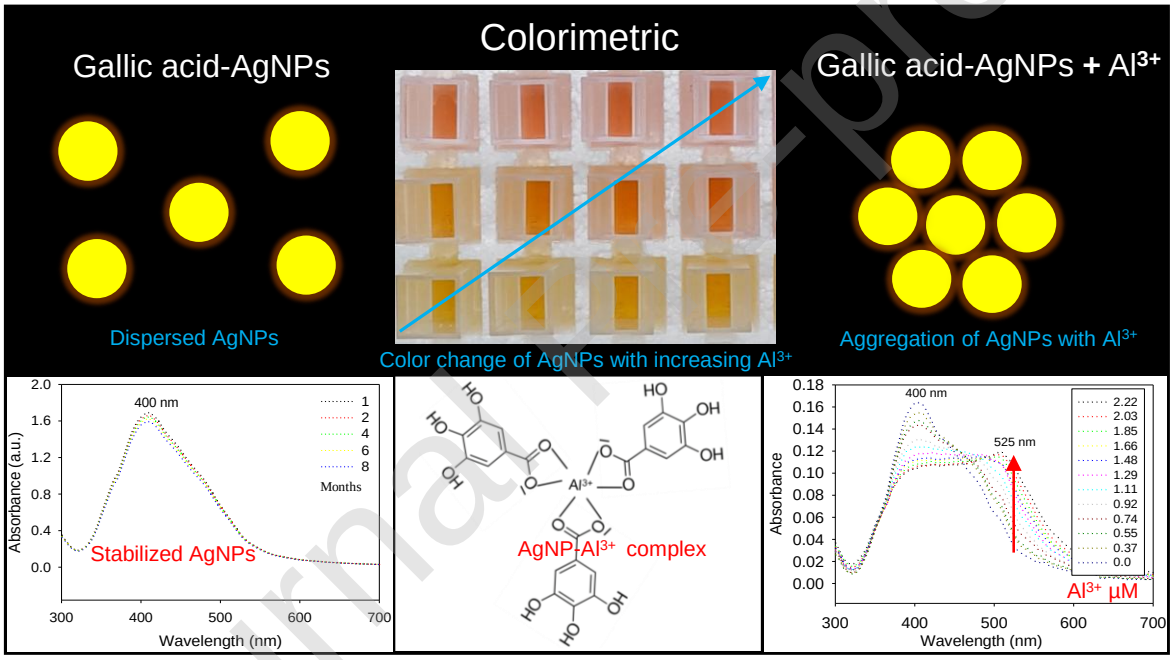

Highlights:

Gallic acid method is most rapid and safe for synthesis of most stable AgNPs

Functional groups of gallic acid showed excellent selectivity and sensitivity for Al^{3+}

High binding affinity of Al^{3+}-phenol complex allows rapid detection and removal of Al^{3+}

AgNPs probe is applicable for monitoring Al^{3+} present in the real water samples

Abstract

Metal chelation-enhanced changes in surface plasmon resonance (SPR) band of gallic acid-functionalized AgNP solution to monitor aluminum ions (Al^{3+}) is reported herein. In aqueous solution, Al^{3+} selectively induced a strong absorbance with large shifts up to ~125 nm from the SPR band with color changing from orange to red. This study illustrates that hydroxyl groups of phenol affect the response of a probe that tunes the absorbance maxima to a longer wavelength at 525 nm. Moreover, the rapid formation of a AgNP-Al^{3+} coordination complex was demonstrated by real-time monitoring, adsorptive removal, and energy dispersive spectroscopy mapping.

Keywords: Gallic acid, Hydroxyl groups, Colloidal solution, Coordination complex, Adsorptive removal

1. Introduction

Increased aluminum salt usage in numerous industrial activities has resulted in the discharge of free aluminum (Al^{3+}) into wastewater [1, 2]. The release of Al^{3+} from cooking utensils that depends on salts and acids such as citric, oxalic, and acetic acids and presence of complexing ligands such as hydroxyl and carboxyl groups [3, 4] is an important issue. In daily life, exposure to traces of Al^{3+} is common owing to the ubiquitous presence of aluminum kitchen wares; meanwhile, acidification in the environment increases the spread of free Al^{3+} cations and can lead to its accumulation in plants and humans [5, 6]. Al^{3+} is a well-known neurotoxin, and even low levels of it can cause behavioral and neuroanatomical changes associated with Parkinson's and/or Alzheimer's disease [7, 8]. The World Health Organization

(WHO) has fixed the permissible limit for Al^{3+} level in drinking water to approximately 200 mg L^{-1} (7.41 μM) [9, 10].

Three main detection methods, namely inductively coupled plasma-mass spectrometry [11], atomic absorption spectrometry [12], and inductively coupled plasma-atomic emission spectrometry, are typically used to detect Al^{3+}. However, sophisticated instruments and methods are complex to operate, expensive, and non-mobile for on-site monitoring of metal ions [13, 14]. Compared with transition metals, the monitoring of Al^{3+} is challenging owing to poor coordination and lack of spectrophotometric characteristics [15]. To the best of our knowledge [16], most reported sensors for Al^{3+} exhibit limitations such as tedious synthetic procedures, low sensitivity, and/or lack of applicability in aqueous solutions [17]. Therefore, colorimetric methods based on gold [18] and silver nanoparticles (NPs) are emerging rapidly to detect metal ions in the aqueous phase, which are visible by naked eyes and suitable for the facile operation and on-site monitoring [19, 20]. In particular, AgNPs are more cost-effective than gold NPs, offering excellent SPR properties, strong and well-defined spectral shifts and ratiometric arrays, and ease of color visualization.

Green tea is rich in polyphenols and phenolic acids including catechin, tannic acid, and gallic acid [21], of which most are well known for their potential metal

chelating activity and preferential binding to hard metals such as Al^{3+} [22]. Furthermore, gallic acid has been reported as a potential reducing and stabilizing agent in the greener synthesis of gold and silver NPs [23, 24]. The gallic acid reduction method has been shown to be rapid and appropriate for the high concentration synthesis of AgNPs, consuming low reaction volume, and lower concentrations of gallic acid [25]. Herein, we report gallic acid-functionalized AgNPs, their comprehensive characterizations, and their use as a colorimetric sensing probe for detecting Al^{3+} with good selectivity and sensitivity.

By UV-vis spectroscopy and X-ray photoelectron spectroscopy (XPS), we discovered that gallic acid could cap the AgNPs that subsequently stabilize by the functional group during the NP growth. This account successfully applied gallic acid-functionalized AgNPs in colorimetric visualization and spectrophotometric monitoring of Al^{3+} in aqueous media. Interaction of Al^{3+} ions with AgNPs exhibited a significant red-shift at absorption λmax of $\sim$525 nm, and energy-dispersive X-ray (EDS) mapping was used to confirm the formation of a coordination complex. Moreover, we investigated the most favorable conditions, pH, and possibilities in monitoring Al^{3+} levels in real-water samples.

2. Materials and Methods

2.1. Chemicals

Silver nitrate ($AgNO_3$) and gallic acid were purchased from Sigma–Aldrich, South Korea. Standard solutions (1,000 ppm) of metal ions were purchased from Kanto Chemicals, Japan and Nacalai Tesque, Japan. Al^{3+} stock solutions (37 μM and 18.5 μM) were freshly prepared by diluting the standard solution. All reagents and chemicals used in these experiments were of analytical grade and used without further purification. Deionized water (DI) was used in the synthesis procedure of the $AgNO_3$ precursors that was performed with fine control of temperature and pH conditions. Furthermore, DI water was used for redispersion after ultracentrifugation was applied to the freshly prepared AgNPs.

2.1.2. Green synthesis of AgNPs

The greener synthesis of AgNPs stabilized by gallic acid was performed according to the procedure by Kim et al. [25]. For synthesis, we used a 20-mM stock solution of $AgNO_3$ and a 12.5-mM solution of gallic acid dissolved in DI water. The alkaline pH condition of the solution was adjusted using 0.1 mL of 1-M NaOH solution. A diluted solution of gallic acid (2.5 mM) was first prepared; subsequently, 1.0 mL of $AgNO_3$ stock solution was quickly injected with vigorous stirring under ambient temperature (22 °C). A rapid formation of AgNPs occurred, as evidenced by a color change in the solution from colorless to yellow and finally, dark brown.

Static temporal evolution of UV-vis spectra of the AgNP solution was monitored at different time intervals (up to 80 min) to confirm the exhaustion of the $AgNO_3$ precursor and quality of the final nanoproduct. After the reduction reaction of the $AgNO_3$ precursor was completed, the solution was stored at room temperature, and the NP solution was processed by ultracentrifugation at 12,000 rpm for 15 min. This allows uncapped gallic acid and added alkaline additives to eliminate, and improves the size distribution of the NPs through a size-selective ultracentrifugal force. Finally, the gallic-acid-functionalized AgNPs were dispersed in DI water and used as a sensitive colorimetric probe for the detection of Al^{3+}.

2.1.3. Characterization of AgNPs

Optical, colloidal, and dilution properties of the gallic acid-functionalized AgNPs were characterized using an Optizen-2120 UV-vis spectrophotometer, from 300 and 700 nm at ambient temperature. XPS measurement was performed on a ULVAC-PHI (Japan/USA) instrument using a monochromatic Al–Kα radiation. The XPS spectra were calibrated against 284.6 eV observed for C1s. The X-ray diffraction (XRD) pattern of a thin film made with AgNPs was obtained using an X-ray diffractometer (Malvern Panalytical Ltd, Malvern, UK) operated at 30 kV and 100 mA. Cu–Kα radiation was used to record the XRD spectrum with a wavelength of 1.5406 Å in the 2θ range of 30–80°. Transmission electron microscopy (TEM)

images were obtained using (FEI Tecnai G^2); samples for TEM imaging were prepared at room temperature by depositing a drop of AgNP solution on a carbon-coated copper grid. Zeta (ζ) potential measurements of the ultracentrifuged AgNP samples were performed in DI water using (Otsuka Electronics, ELS 8000).

2.2. Sensing of Al^{3+}

2.2.1 Selectivity

Absorption spectra of the AgNPs in the presence of individual metal ions (Al^{3+}, Mg^{2+}, Co^{2+}, Cr^{3+}, Hg^{2+}, Pb^{2+}, Ge^{2+}, As^{+}, Bi^{3+}, Mn^{2+}, K^{+}, Ca^{2+}, Na^{+}, Zn^{2+}, Ba^{2+}, Cd^{2+}, Mo^{2+}, Ni^{2+}, Pt^{2+}, Y^{+}, Se^{2+}, Pd^{2+}, and Cs^{+}, 200 ppb) and PO^{3-}, NH_4, and NO^{3-} were tested at ambient temperature. To investigate the selectivity, the gallic acid AgNPs were mixed separately with different metal ions and equilibrated for 5 min before color and spectral measurements.

2.2.2 Determination of standard solution of Al^{3+}

A quantitative determination of Al^{3+} was performed in aqueous solution for both narrow and broad concentration ranges. Various concentrations of Al^{3+} for the narrow range were prepared using 0.1 mL of the stock AgNPs: 0.37, 0.55, 0.74, 0.92, 1.11, 1.29, 1.48, 1.66, 1.85, 2.03, and 2.22 µM Al^{3+}. Meanwhile, various concentration of Al^{3+} for the broad range were prepared using 0.4 mL of the stock

AgNPs: 0.37, 0.74, 1.18, 2.22, 2.96, 3.70, 4.44, 5.18, 5.93, 6.67, 7.41, 8.15, and 8.89 μM Al^{3+}. The final volume of the probe solutions (1 mL) was adjusted by adding the appropriate amount of DI water. The sensor solutions were equilibrated for 5 min before spectral measurements in the range of 300 to 700 nm.

2.2.3. Effect of pH

The effect of pH was studied as follows: 0.2 mL of the AgNP stock solution was suspended in DI water at either pH 5, 6, 7, 8, or 9. Subsequently, the suspension was left for 5 min, and the absorbance of the suspensions was measured at 400 and 525 nm. Al^{3+} (4.44 μM) was subsequently added. The suspension was left for another 5 min, and the absorbance was measured again at 400 and 525 nm.

2.2.4. Real-time response of AgNPs to Al^{3+}

The real-time spectral response of the AgNPs was performed at 4.44 μM Al^{3+} as follows: 0.2 mL of AgNP stock solution was suspended in DI water. The absorbance at 400 and 525 nm was subsequently recorded at various times (from 1 to 10 min). A long-term absorbance response (30 min to 720 min) of the AgNP solution was observed for Al^{3+} at increasing concentrations from 0.37 to 8.89 μM. The absorbance changes and real-time decay profiles of the AgNP solutions were recorded at both 400 and 525 nm.

2.2.5. Interference and sedimentation

Al^{3+} aqueous solutions and other metal ion solutions were freshly prepared and used for interference study. The interference to gallic-acid AgNP probe while detecting Al^{3+}, with the competing metal ions (Mg^{2+}, Co^{2+}, Cr^{3+}, Hg^{2+}, Pb^{2+}, Ge^{2+}, As^{+}, Bi^{3+}, Mn^{2+}, K^{+}, Ca^{2+}, Na^{+}, Zn^{2+}, Ba^{2+}, Cd^{2+}, Mo^{2+}, Ni^{2+}, Pt^{2+}, Y^{+}, Se^{2+}, Pd^{2+}, and Cs^{+}), was investigated with 1.0 equivalent of Al^{3+} in the presence of other ions (4.0 equivalent). The AgNP Al^{3+} coordination complexes formed with the other metal ions were maintained at ambient temperature for 12 h, and their UV-vis absorbance spectra were recorded using a spectrophotometer.

2.2.6. Removal of Al^{3+} from aqueous solutions

The ability of AgNPs in removing Al^{3+} from the aqueous solutions were investigated as follows: 0.4 mL of AgNPs stock solution was added to water. Subsequently, 4.44, 5.18, 5.93, 6.67, 7.41, 8.15, and 8.89 µM Al^{3+} was added to the abovementioned solution and remained static. The fate of the Al^{3+}-bound AgNP aggregates was monitored by UV-vis spectroscopy for 12 h and subsequently observed for color and sedimentation.

2.2.7. Application of AgNPs in real-water samples

Real-water samples were collected from the tap of the laboratory, lake, river, and wastewater treatment plant and tested to verify the possibility of Al^{3+} on-site monitoring and identify any interferences from unknown pollutants. These water samples were first filtered using Whatman paper and subsequently spiked with the appropriate amount of Al^{3+} from the stock solution. The concentrations of Al^{3+} in these samples were subsequently determined using inductively coupled plasma mass spectroscopy (ICP-MS) and standard graph prepared for Al^{3+} using the gallic acid-functionalized AgNPs.

3. Results and Discussion

3.1. Synthesis of gallic-acid-stabilized AgNPs

To observe the NP growth process, small amounts of solutions from the reaction were analyzed directly by UV-vis absorption spectroscopy at various reaction times (Fig. 1a). The intensity of the SPR band improved significantly within 5 to 10 min of incubation and subsequently reached a maximum in a total reaction time of approximately 80 min, without any signs of red-shift (Fig. 1a). The SPR bandwidths of the AgNP solution indicated a narrow size distribution of AgNPs in solution, as shown in (Fig. 1a). Ag^{+} was reduced in the aqueous medium and enabled a characteristic SPR peak between 390–420 nm to developed, thus revealing the

fabrication of the AgNPs. Additionally, we observed no decrease in both the SPR intensity and aggregation of the freshly formed AgNPs. According to Figs. 1a,b, the NP shape remains spherical until the end of the reaction times; meanwhile, changes in the size with increasing reaction time should induce a red-shift in the SPR band. The absorbance intensity of the AgNPs was monitored at 420 nm and plotted as a function of time; the corresponding photographs of the AgNP solutions are presented in the inset of Fig. 1b. The UV-vis spectra evolution of the AgNPs continued for a short time (~20 min) as both the $AgNO_3$ precursor depleted rapidly and the newly formed AgNPs matured completely. The reduction of $AgNO_3$ and growth of AgNPs that occurred at the alkaline pH condition were consistent with the well-known growth theory, i.e., classical nucleation and nanoparticle growth [26].

The stability of the AgNPs in DI was further evaluated by ζ potential measurement. The ζ potential value of the AgNPs was approximately -48.8 in DI water (data not shown); this demonstrates the high stability level of colloidal systems produced using gallic acid. Gallic acid, therefore, plays a passivation role during the nucleation of Ag atoms and AgNP growth. This type of surface passivation may allow the use of metal, oxides, and semiconductor NPs in a variety of different applications while maintaining the inherent properties of the core particles [27]. It appears that gallic acid, with its high complexation capacity toward Ag^+, can result

in the rapid nucleation and growth of Ag nuclei, thus forming mature AgNPs with a narrow size distribution [28]. Metal NPs that readily oxidize or aggregate in solution owing to physical and surface chemistry render them unsuitable for practical applications [29].

The gallic acid-functionalized AgNPs enable the stability of the SPR band and the optical properties of the NPs to be sustained over a long period when the samples were stored at room temperature (Fig. 1c). In our case, gallic acid not only allowed a rapid synthesis but also caused a stable dark yellow-colored colloidal dispersion of AgNPs to form; furthermore, it did not affect both the color and SPR band for 8 to 12 months (Fig. 1c). It is well known that the aggregation-prone nature of NPs could cause slow or rapid degradation of the SPR band. Thus, the colloidal stability of metal NPs is an important factor in application development [30].

The aqueous phase of the AgNPs was used to demonstrate the facile separation of unreacted $AgNO_3$ and gallic acid in the synthesis by ultra-centrifugation. We observed that the optical and structural properties of AgNPs were not affected by ultracentrifugation; thus, gallic acid resulted in a high degree of stability, allowing pellet dispersion and sample storage for a longer period at room temperature (Fig. 1d). As the production of dispersed NPs is vital to ensure the reliability of NPs in biological and analytical applications [31], we investigated the

effect of ultracentrifugation techniques on the purification and dispersal of gallic acid-functionalized AgNPs.

3.1.1 Characterization of AgNPs

We used XRD and XPS to reveal the chemical composition and crystalline nature of the AgNPs, as shown in Fig. 2. The XPS spectra indicate the presence of silver, carbon, oxygen, and nitrogen, thus suggesting the successful synthesis and capping of gallic acid onto the AgNPs (Fig. 2a). XPS analysis provided essential information regarding the oxidation states of elements and surface bonding on the AgNP surfaces. The AgNPs were further described by a high-resolution XPS, and the Ag3d core levels of the AgNP thin films are shown in Fig. 2b. The Ag3d XPS spectra of the AgNPs indicate the presence of two spin-orbit pair components. The main $Ag3d_{5/2}$ signal component was centered at 367.8 eV binding energy, thus clearly suggesting the firm structure of silver atoms in the AgNPs. The second spin-orbit pair component of the AgNPs was established with a lower intensity and observed at larger BE values ($Ag3d_{3/2}$ at 373.8 eV); thus, the NPs were predictable owing to more surface Ag atoms binding to the gallic acid molecules through OH–(AgNP–OH–) [32].

The representative XRD spectra of the AgNP thin film, as shown in Fig. 2c, illustrate the cubic structures of silver, with distinct peaks at 37.9°, 44.2°, 64.3°, and

77.2° corresponding to (111), (200), (220), and (311) lattice planes, respectively. The classical Scherrer equation suggests an average crystallite diameter of AgNPs of ~21 nm that is larger than the average size (14 nm) obtained by TEM image analysis (Fig. 2d). The TEM images of the AgNPs revealed a spherical morphology without any signs of aggregation and their size varying from 5 to 20 nm. The hydrodynamic diameter of the AgNPs was determined by dynamic light scattering measurements (data not shown), and the results revealed an average diameter of 18 nm with a relatively narrow size distribution that agrees with both the TEM and XRD results.

3.2. Sensing results

3.2.1. Selectivity

It has been suggested that oxygen-containing functional groups on NPs exhibit a high affinity for metal ions, particularly electropositive ones [33]. Hence, we synthesized AgNPs using gallic acid, which contains abundant hydroxyl groups, to demonstrate high selectivity toward Al^{3+}. The selectivity of the AgNPs was tested under identical pH and temperature conditions (22 °C) and revealed that this probe exhibits a characteristic spectral response for Al^{3+} as compared with other ions including Mg^{2+}, Co^{2+}, Cr^{3+}, Hg^{2+}, Pb^{2+}, Ge^{2+}, As^{+}, Bi^{3+}, Mn^{2+}, K^{+}, Ca^{2+}, Na^{+}, Zn^{2+}, Ba^{2+}, Cd^{2+}, Mo^{2+}, Ni^{2+}, Pt^{2+}, Y^{+}, Se^{2+}, Pd^{2+}, and Cs^{+}, 200 ppb) (Figs. 3a, b). The

spectral response of the AgNPs to Mg^{2+} Pt^{2+} and Cr^{3+} was unique with a minor blue-shift of the SPR band and significant enhancement of the SPR band intensity (Figs. 3a, b).

Figure 3c, d shows the differences in absorbance at 525 nm for AgNP-based detection systems that are incubated under identical conditions with various metal ions. The inset of Fig. 3c shows a digital photograph of the AgNPs incubated with various metal ions under identical conditions; it suggests the development of a dark red color only for the Al^{3+} ions. As shown in the inset of Fig. 3c, the AgNPs were orange and green for Mg^{2+} and Pt^{2+}, respectively, without any characteristic red-shift toward larger wavelengths. As shown in (Figs. 3a, b), possibilities in the detection of Cr^{3+}, Mg^{2+}, and Pt^{2+} warrants further investigation. This study is focused exclusively on the development of an effective and practical sensing probe for Al^{3+} at ambient temperature. The AgNPs exhibited good selectivity and high sensitivity to Al^{3+}, with a color change from dark yellow to red, as shown in the inset of Fig. 3c. This is supported by the characteristic red-shift at 525 nm (Fig. 3a) as well. A sensitive and selective colorimetric sensing method based on glutathione-modified silver AgNPs was recently reported for the analysis of Co^{2+} ions [34].

3.2.2. Sensitivity of gallic-acid AgNPs to Al^{3+}

Both narrow and broad concentration ranges were used to validate the practical quantification of Al^{3+} using a gallic acid-functionalized AgNP solution. Changes in the SPR band intensity and position of the red-shifted peak of the AgNPs were examined using UV-vis spectroscopy after 5 min of incubation with increasing concentrations of Al^{3+} (Fig. 4). The SPR intensity of the AgNPs in the presence of Al^{3+} ions was lower than that in the absence of Al^{3+}. The intensity of the SPR peak at 400 nm decreased linearly with increasing Al^{3+} concentration, with the formation of a new peak at 525 nm (Fig. 4a). Thus, changes in the absorbance intensities at these two wavelengths were chosen to quantify Al^{3+}. Measurements of Al^{3+} over a narrow concentration range were performed by adding increasing concentrations of Al^{3+} (from 0.37 to 2.22 µM) to solutions of AgNPs (Figs. 4b,c). The plot of Al^{3+} at concentrations ranging from 0.37 to 2.22 µM revealed a linear correlation; the value of the linear regression coefficients (R^2) were 0.94 and 0.98 for the absorbance at 400 and 525 nm, respectively (Figs. 4b,c). A color change in the AgNPs from dark yellow to reddish-brown was observed for both the narrow and broad concentration ranges of Al^{3+}, as shown in the inset of Figs. 4 a,d. Compared with previously reported methods (Table 1), this method can provide a rapid analysis of trace amounts of Al^{3+} with excellent sensitivity and selectivity at ambient temperature and neutral pH conditions. The limit of detections (LODs) of the newly established method was calculated to be 0.92 µM visually and 0.55 µM using UV-vis

spectroscopy. Meanwhile, other methods yielded lower values, e.g., those based on the fluorescent properties of benzothiazole (2.2 μM μM) [35], chemosensor (3.3 μM) [36], and colorimetric sensor based on polyacrylate (2.0 μM) [37]. Therefore, the visually determined LOD was found to be adequate to establish a sensitive, selective, and practical probe for the quantitative detection of Al^{3+} at micromolar levels in the aqueous phase.

The potential to measure a broad concentration range of Al^{3+} (0.37 to 8.89 μM) is presented in Fig. 4d. A linear response is shown in the absorbance intensity of the characteristic peaks at 400 nm and 525 nm of the AgNPs from Al^{3+} concentrations of 0.74 and a higher concentration of Al^{3+} (Figs. 4e, f). The values of the absorbance intensities observed at 400 nm and 525 nm are plotted for Al^{3+} concentrations ranging from 0.37 to 8.89 μM, and these values exhibited a linear response as a function of Al^{3+} concentration (Figs. 4e, f). A highly sensitive and selective colorimetric probe for Al^{3+} species exhibited ratiometric responses in an aqueous medium by the formation of the aggregated form of AgNPs. Our results further confirm the impressive LOD determined in the broad concentration range: ~3.7 μM visually and the spectral LOD of Al^{3+} of ~1.48 μM. The LOD values obtained are considerably lower than the upper limit of 7.41 μM proposed by the WHO for Al^{3+} in drinking water [10]. A similar linear trend for the detection of Al^{3+} using tannic-

acid-capped gold NPs and a benzothiazole-based fluorescent probe [35, 38] has been reported. In recent years, the quantitative detection of Al^{3+} with a linear correlation from 0.5 to 10 ppm using indole-2-carboxylic acid-stabilized AgNPs [39] has been reported.

3.2.3. Effect of pH

The colorimetric and spectral changes occur owing to metal-ligand interactions through the coordination chemistry of hydroxyl functional groups on the surface of the AgNPs with Al^{3+}. Therefore, we measured the absorbance intensity of the AgNPs between pH 5 to 8 in the presence and absence of Al^{3+} (Fig. 5a). At low pH values, the color change from yellow to red was not observed owing to the protonation of the functional groups; however, neutral and high pH values readily supported the formation of AgNPs aggregates. Similarly, a slight decrease in absorbance intensity at 525 nm under basic conditions (pH > 9) was shown owing to increased deprotonating, which partly impaired the complexation of Al^{3+} with the hydroxyl groups. These results suggest that the maximal complexation of the AgNPs and Al^{3+} occurs around neutral pH (Fig. 5a). Hydroxyl groups assist with the formation of pH-dependent insoluble polyphenol-Al^{3+} complexes; furthermore, it has been suggested that complexes are predominant at pH 7 [40], which is consistent with our observations. A naphthalene-derivate-based fluorescent probe

demonstrated high selectivity at pH 7 while detecting Al^{3+} in water [41]. It is well known that probes based on electron donor/acceptor interactions typically result in the poor sensitivity and recognition of target metal ions by the interference of protons in the sensing medium [42].

3.2.4. Real-time response of AgNPs to Al^{3+}

The time course of the decrease in intensity of the absorbance at 400 nm and the increase in the intensity of absorbance at 525 nm were monitored in the presence of 4.44-µM Al^{3+} (Fig. 5b). The change in the absorbance pattern indicated the rapid binding of Al^{3+} to the AgNPs; thus, the signal can be achieved immediately after the exposure of Al^{3+}. After adding the aqueous solution of Al^{3+} to the AgNP solution, the absorbance intensity at 400 nm reached a minimum value within 120 s (Fig. 5b). It subsequently remained nearly stable for up to 10 min, indicating that a 5-min incubation is optimal for monitoring Al^{3+}-induced aggregations of the AgNPs. Generally, most chemosensors developed hitherto require long response times (see Table 1 and [43]. However, in our study, we discovered the rapid binding of Al^{3+} to AgNPs. The gallic acid moieties coated on the AgNPs were most reactive toward Al^{3+}; this can be attributed to the higher rate of the coordination chemistry that enables the rapid detection of Al^{3+}, as reported previously [44]. Repeated experiments revealed that the developed probe is novel in terms of rapid response,

thus signifying a potential ‘‘zero-wait’’ method for detecting Al^{3+}, as suggested in a recent report [37].

Additionally, real-time spectral measurements were performed within 30 to 1440 min at four different Al^{3+} concentrations (0.74, 2.96, 3.70, and 4.44 μM). The absorbance intensity of the red-shifted band increased gradually as the reaction time progressed with Al^{3+} (0.74 μM), indicating the possible formation of unstable AgNP aggregates (Fig. S1a). The fractal growth of the AgNP aggregates was reflected as a gradual increase in absorbance at 525 nm after a reaction with Al^{3+} (2.96 and 3.70 μM) (Fig. S1b). The red-shifted band appeared within 180 min owing to the size increase of the AgNP aggregates with Al^{3+} (2.96 and 3.70 μM) (Fig. S1c). The decline in absorbance at higher Al^{3+} (4.44 μM) began much later at ~360 min, thus indicating that the timing of the probe was acceptable for practical applications (Fig. S1d). The aggregative behavior of the gallic-acid-functionalized AgNPs was progressive in the coordination reaction.

Further experiments were performed to explore the decay profiles of the absorbance intensity as a function of time (min) over a broad concentration range of Al^{3+} (0.37 to 8.89 μM). The absorbance signal was found to be linearly proportional across the broad Al^{3+} concentration range within 10 to 30 min of coordination reaction. However, the decay pattern of the observed absorbance remained

dependent on the Al^{3+} concentration, as detected in real-time absorbance measurements (Fig. 6). The observed absorbance intensity at 400 nm shows that the absorbance initially decreased rapidly and subsequently underwent a more gradual further decrease as a function of time (Fig. 6a). The AgNP-Al^{3+} complex that was formed with 3.70-μM Al^{3+} increased the absorbance intensity at 525 nm up to 180 min and subsequently entered a stationary phase up to 480 min. A linear increase in absorbance intensity at 525 nm was observed within 180 min for the reaction of 4.44-μM Al^{3+} followed by a declining phase without the sign of a stationary phase (Fig. 6b). The sedimentation of AgNP aggregates caused the rapid decay of the absorbance intensity, as evidenced in suspensions from 5.18 to 8.89 μM Al^{3+}; this is because bulk AgNPs tend to settle owing to gravity.

3.2.5. Analysis of real-water samples

Al^{3+}-chelating effects of hydroxyl groups [40] and their importance in Al^{3+} detoxification and plant growth [45] have been reported. High levels of Al^{3+} in the brain have been reported to cause dementia, and a range of neurological disorders [46]. Thus, it would be highly desirable to test the applicability of the newly designed sensing platform to detect Al^{3+} in real-water samples from the tap, lake, river, and wastewater sites that contain various metal ions and unknown contaminants. In a practical assay, we collected samples of tap water from the laboratory, local lake,

river, and wastewater and filtered them through Whatman paper to remove any suspended particles. The Al^{3+} content of the spiked water samples was subsequently measured using a calibration curve; the results are presented in Table 2, along with the results from ICP-MS measurements. Except for the wastewater sample, the results obtained (Table 2) reflect the added amount of Al^{3+}, thereby validating the feasibility of the developed method for practical applications. Thus, this colorimetric method, which can be perceived by the naked eye, is an appropriate method for the real-time detection of target Al^{3+} ions owing to its simple operation and on-site convenience.

3.2.6. Interference study

Low interference is vital for the validation of an excellent sensor [47]. Therefore, interference in the detection of Al^{3+} was investigated by testing its response to 1.0 equivalent of Al^{3+} in the presence of other ions (4.0 equivalent) under identical conditions. In this case, we used a wide range of metal ions: Mg^{2+}, Co^{2+}, Cr^{3+}, Hg^{2+}, Pb^{2+}, Ge^{2+}, As^{+}, Bi^{3+}, Mn^{2+}, K^{+}, Ca^{2+}, Na^{+}, Zn^{2+}, Ba^{2+}, Cd^{2+}, Mo^{2+}, Ni^{2+}, Pt^{2+}, Y^{+}, Se^{2+}, Pd^{2+}, and Cs^{+} as interfering ions. The experimental results, shown in Figs. S2a, b, indicate that the absorbance intensities of the AgNPs were slightly affected at 400 nm; however, spectral shifts were not observed despite the presence of a wide range of other metal ions, as shown in Figs. S2a, b. As the presence of Pt^{2+}

and Mg^{2+} prevented the formation of red-shift that typically occurs in the presence of Al^{3+}, we did not expect interference to occur (Figs. S2b, c). Meanwhile, the results indicate that the other metal ions did not interfere with the formation of spectral shifts toward larger wavelengths, although the intensity at 525 nm varied slightly (Figs. S2b, c). This result suggests the use of hydroxyl groups to form coordination complexes with Mg^{2+} without any interference from other cations such as Ca^{2+} and K^{+}, which agrees with that of a previous study [48]. Additionally, the removal of heavy metal ions from aqueous media has been reported to reveal the possible adsorption mechanism of 8-hydroxyquinoline-functionalized multiwalled carbon nanotubes [49].

3.2.7. Removal of Al^{3+} from water

Recent findings suggest that aluminum in drinking water is a risk factor for Alzheimer's disease [50]. Therefore, simultaneous detection and recovery of Al^{3+} from the water was tested using surface ligands of the AgNPs. AgNPs from stock solutions were added to Al^{3+} solutions ranging from 0.37 to 8.89 µM and observed for up to 12 h while they remained static at ambient temperature (Figs. S3(a-d)). Subsequently, sedimentation was performed to separate the Al^{3+}-bound AgNP complexes from the reaction solution, as shown in the Supplementary Materials. As indicated by the inset of Fig. S3a, the solution turns to red almost immediately after

Al^{3+} was mixed into the solution. The spectral profile of the AgNPs treated with increasing concentrations of Al^{3+} (4.44 to 8.889 μM) is presented to track the changes in red-shifted UV-vis spectra (Figs. S3b, c). Sedimentation was performed to separate the Al^{3+}-bound probe from the aqueous solution after 12 h. The solution became clear and colorless (Fig. S3d), indicating the applicability of the AgNPs for removing Al^{3+} from the water samples. Moreover, the AgNPs used as a colorimetric probe could be used in removing Al^{3+} with the assistance of the sedimentation process; thus, secondary pollution could be avoided. Intrinsic–OH and –OH groups are known as prominent reaction sites that can complex metals ions in solution and are useful for the preconcentration or extraction of metal ions [51]. Similarly, removal of Al^{3+} from water and industrial wastewater by magnetic nanoparticles has been reported [52].

3.2.8. Morphological and elemental analysis of AgNP-Al^{3+} complexes

We performed TEM imaging to observe the size and distribution of the gallic acid-functionalized AgNPs in aqueous solution before and after the addition of Al^{3+}. Fig. 7(left side) shows the TEM image and morphology of the AgNPs, in which each particle is well distinguished and monodispersed in the aqueous media. Fig. 7(right side) shows the TEM image of aggregated AgNPs after the addition of Al^{3+}; they could not be well distributed owing to the agglomeration of the AgNPs. The size of

the AgNPs treated with Al^{3+} was found to be larger than that of the monodispersed NPs. The average diameter and size distribution analysis of the AgNPs presents a significant difference in NP properties before and after the addition of Al^{3+}. A 20-fold increase in the size of the aggregated AgNPs with Al^{3+} was observed as compared with that of monodispersed AgNPs. In particular, the AgNPs offer excellent SPR properties, in addition to exhibiting strong and well-defined color that eased visualization, as shown in the inset of Fig. 7. Meanwhile, the colorimetric detection method for the detection of Al^{3+} based on a new aggregation mechanism of etched AgNPs has been reported recently [44]. Additionally, a colorimetric probe for the detection of Al^{3+} based on 11-mercaptoundecanoic acid-functionalized gold nanoparticles has been reported, in which the results confer to the chelation effect amid the carboxyl group and Al^{3+} [53].

The EDS drift-corrected spectra of Al^{3+} coordinated AgNPs shown in Fig. 8b reveal the presence of only Ag, Al, O, and C elements. The selected area of AgNP aggregates in the TEM image for Al^{3+} (3.70 μM) is shown in Figs. 8c, d. The uptake of Al^{3+} by the AgNPs was confirmed by EDS elemental mapping, as presented in Figs. 8e, f. The AgNPs were aggregated after the treatment; the EDS mapping results indicate that Al^{3+} can be removed from the reaction mixture. As the main constituent metals of AgNP aggregates, Figs. 8e, f show the corresponding Al^{3+} and Ag EDS

maps. The EDS mapping data show that Al^{3+} was distributed around the surface of the AgNPs, ultimately covering the entire surface of the AgNPs (Figs. 8e, f). As shown, the distribution of Al^{3+} on the AgNP surface is relatively homogeneous (Fig. 8e). The mapping result suggests that the AgNP surface participated in the coordination reaction and subsequently accelerated the agglomeration of AgNPs. Furthermore, the EDS results confirmed the role of AgNPs for the removal of Al^{3+}. This study demonstrates the simultaneous detection and capturing of Al^{3+} using ligands on the AgNPs; similarly, a previous report demonstrated the detection and sorption of Pd(II) using ligands immobilized onto meso-adsorbents [54].

4 Conclusions

Spherical gallic acid-functionalized AgNPs were prepared and comprehensively evaluated for the colorimetric and spectrophotometric detection of Al^{3+} in an aqueous medium. The hydroxyl group in gallic acid exhibits an affinity to metal ions; thus, several metallic cations were selected to test the selectivity and interference. The colorimetric sensing of Al^{3+} was based on the fact that AgNPs underwent aggregation immediately after the formation of a chelating complex between Al^{3+} and –OH groups, thereby resulting in a red-shifted SPR band at 525 nm that produced a distinct color change from yellow to red. The results clarified

that the colorimetric detection and adsorption of Al^{3+} onto the AgNP surface were dependent on the initial Al^{3+} concentrations, contact time, and solution pH. More importantly, the observed spectral LOD of 0.55 µM and the visual LOD of approximately 0.92 µM were significantly lower than that of the upper limit (Al^{3+}, 7.41 µM) in drinking water recommended by the U.S. EPA and WHO. In particular, the advantages of this new route include ease of synthesis and stabilization, high level of speed, and the non-requirement for sophisticated equipment for on-site monitoring.

Conflict of interest:

The authors do not have any conflicts of interest to declare.

Acknowledgments

The Dongguk University-Seoul Research Fund 2018-2020 also supported this research. The authors also would like to extend their sincere appreciation to King Saud University, Deanship of Scientific Research, College of Sciences Research Centre, for supporting this research.

References

[1] J.C. Wesdock, I.M.F. Arnold, J. Occup. Environ. Med. 56 (2014) S5-S11.

[2] C. Exley, Environ. Sci. Process. Impacts,15 (2013) 1807-1816.

[3] A.D. Semwal, A. Padmashree, M.A. Khan, G.K. Sharma, A.S. Bawa, J. Sci. Food Agric. 86 (2006) 2425-2430.

[4] L.A. Al Juhaiman, J. Saudi Chem.Soc. 14 (2010) 131-137.

[5] J. Zhang, Z. Lyu, S. Shao, F. Li, S. Yang, W. Song, W. Li, S. Li, Chin. Geogr. Sci. 26 (2016) 495-507.

[6] S.J. Zheng, Ann. Bot. 106 (2010) 183-184.

[7] M. Kawahara, M. Kato-Negishi, Int. J. Alzheimers Dis. 2011 (2011) 276393.

[8] S.C. Bondy, Neuro Toxicol. 52 (2016) 222-229.

[9] J.-B. Liu, W. Wang, G. Li, R.-X. Wang, C.-H. Leung, D.-L. Ma, ACS Omega, 2 (2017) 9150-9155.

[10] T. Han, X. Feng, B. Tong, J. Shi, L. Chen, J. Zhi, Y. Dong, Chem.Comm. 48 (2012) 416-418.

[11] A. Sanz-Medel, A.B. Soldado Cabezuelo, R. Milačič, T. Bantan Polak, Coord. Chem. Rev. 228 (2002) 373-383.

[12] M.H. Mashhadizadeh, M. Amoli-Diva, J. Anal. Atom. Spectrom. 28 (2013) 251-258.

[13] M. Frankowski, A. Zioła-Frankowska, I. Kurzyca, K. Novotný, T. Vaculovič, V. Kanický, M. Siepak, J. Siepak, Environ. Monit. Assess. 182 (2011) 71-84.

[14] A.M. Asiri, M.M. Hussain, M.N. Arshad, M.M. Rahman, J. Ind. Eng.Chem. 63 (2018) 312-321.

[15] S.M. Hossain, A. Lakma, R.N. Pradhan, A. Chakraborty, A. Biswas, A.K. Singh, RSC Advances, 5 (2015) 63338-63344.

[16] S.H. Kim, H.S. Choi, J. Kim, S.J. Lee, D.T. Quang, J.S. Kim, Org. Lett. 12 (2010) 560-563.

[17] W. Lin, L. Yuan, J. Feng, Eur. J. Org. Chem. 2008 (2008) 3821-3825.

[18] E.M.S. Azzam, A.F.M. El-farargy, A.A. Abd-Elaal, J. Ind. Eng. Chem. 20 (2014) 3905-3912.

[19] U. Jeong, Y. Kim, J. Ind. Eng. Chem.31 (2015) 393-396.

[20] K. Singh, D. Kukkar, R. Singh, P. Kukkar, K.-H. Kim, J. Ind. Eng. Chem. (2018).

[21] Y. Mizukami, Y. Sawai, Y. Yamaguchi, J. Agric. Food Chem. 55 (2007) 4957-4964.

[22] M.n. Ó'Coinceanainn, M.J. Hynes, J. Inorg. Biochem. 84 (2001) 1-12.

[23] D.-Y. Kim, M. Kim, S. Shinde, J.-S. Sung, G. Ghodake, Colloids Surf. B 149 (2017) 162-167.

[24] D. Li, Z. Liu, Y. Yuan, Y. Liu, F. Niu, Process Biochem. 50 (2015) 357-366.

[25] D.-Y. Kim, J. Suk Sung, M. Kim, G. Ghodake, Mat. Lett.155 (2015) 62-64.

[26] J. Polte, Cryst. Eng. Comm. 17 (2015) 6809-6830.

[27] D.-S. Park, H. Wang, S.K. Vasheghani Farahani, M. Walker, A. Bhatnagar, D. Seghier, C.-J. Choi, J.-H. Kang, C.F. McConville, Sci. Rep. 6 (2016) 18449.

[28] J.I. Hussain, A. Talib, S. Kumar, S.A. Al-Thabaiti, A.A. Hashmi, Z. Khan, Colloids Surf. A 381 (2011) 23-30.

[29] C.-N. Lok, C.-M. Ho, R. Chen, Q.-Y. He, W.-Y. Yu, H. Sun, P.K.-H. Tam, J.-F. Chiu, C.-M. Che, J. Biol. Inorg. Chem. 12 (2007) 527-534.

[30] T.L. Moore, L. Rodriguez-Lorenzo, V. Hirsch, S. Balog, D. Urban, C. Jud, B. Rothen-Rutishauser, M. Lattuada, A. Petri-Fink, Chem. Soc. Rev. 44 (2015) 6287-6305.

[31] J.D. Robertson, L. Rizzello, M. Avila-Olias, J. Gaitzsch, C. Contini, M.S. Magoń, S.A. Renshaw, G. Battaglia, Sci. Rep. 6 (2016) 27494.

[32] I.E. dell'Erba, C.E. Hoppe, R.J.J. Williams, Langmuir, 26 (2010) 2042-2049.

[33] R. Azadbakht, J. Khanabadi, Tetrahedron, 69 (2013) 3206-3211.

[34] H. Lee, H.K. Sung, C. Park, Y. Kim, J. Ind. Eng. Chem. 48 (2017) 235-241.

[35] Y. Chen, T. Wei, Z. Zhang, T. Chen, J. Li, J. Qiang, J. Lv, F. Wang, X. Chen, Ind. Eng. Chem. Res. 56 (2017) 12267-12275.

[36] W. Cao, X.-J. Zheng, J.-P. Sun, W.-T. Wong, D.-C. Fang, J.-X. Zhang, L.-P. Jin, Inorg. Chem. 53 (2014) 3012-3021.

[37] A. Kumar, M. Bhatt, G. Vyas, S. Bhatt, P. Paul, ACS Appl. Mater. Interfaces, 9 (2017) 17359-17368.

[38] A.L. Suherman, E.E.L. Tanner, S. Kuss, S.V. Sokolov, J. Holter, N.P. Young, R.G. Compton, Sensor Actuat B-Chem. 265 (2018) 682-690.

[39] P. Joshi, R. Painuli, D. Kumar, ACS Sustain. Chem. Eng. 5 (2017) 4552-4562.

[40] L. Zhang, R. Liu, B.W. Gung, S. Tindall, J.M. Gonzalez, J.J. Halvorson, A.E. Hagerman, J. Agric. Food Chem. 64 (2016) 3025-3033.

[41] Z. Liu, Y. Li, Y. Ding, Z. Yang, B. Wang, Y. Li, T. Li, W. Luo, W. Zhu, J. Xie, C. Wang, Sensor Actuat B-Chem. 197 (2014) 200-205.

[42] M. Shyamal, P. Mazumdar, S. Maity, G.P. Sahoo, G. Salgado-Morán, A. Misra, J. Phys. Chem. A 120 (2016) 210-220.

[43] A.K. Saini, V. Sharma, P. Mathur, M.M. Shaikh, Sci. Rep. 6 (2016) 34807.

[44] N. Yang, Y. Gao, Y. Zhang, Z. Shen, A. Wu, Talanta, 122 (2014) 272-277.

[45] T. Okuda, W. Nishijima, M. Sugimoto, N. Saka, S. Nakai, K. Tanabe, J. Ito, K. Takenaka, M. Okada, Water Res. 60 (2014) 75-81.

[46] D.R.C. McLachlan, C. Bergeron, P.N. Alexandrov, W.J. Walsh, A.I. Pogue, M.E. Percy, T.P.A. Kruck, Z. Fang, N.M. Sharfman, V. Jaber, Y. Zhao, W. Li, W.J. Lukiw, Molecular Neurobiology, 56 (2019) 1531-1538.

[47] S. Chen, Y.-M. Fang, Q. Xiao, J. Li, S.-B. Li, H.-J. Chen, J.-J. Sun, H.-H. Yang, Analyst, 137 (2012) 2021-2023.

[48] D.-Y. Kim, S. Shinde, G. Ghodake, J. Colloid Interface Sci. 494 (2017) 1-7.

[49] M. Abdel Salam, G. Al-Zhrani, S.A. Kosa, J. Ind. Eng. Chem. 20 (2014) 572-580.

[50] V. Rondeau, D. Commenges, H. Jacqmin-Gadda, J.F. Dartigues, Am. J. Epidemiol. 152 (2000) 59-66.

[51] M. Ghaedi, M. Montazerozohori, N. Rahimi, M.N. Biysreh, J. Ind. Eng. Chem. 19 (2013) 1477-1482.

[52] R. Asrarian, R. Jadidian, H. Parham, S. Haghtalab, Adv. Mater. Res. 829 (2014) 752-756.

[53] R. Zhu, J. Song, Q. Ma, Y. Zhou, J. Yang, S. Shuang, C. Dong, Anal. Methods, 8 (2016) 7232-7236.

[54] M.R. Awual, M.A. Khaleque, Y. Ratna, H. Znad, J. Ind. Eng. Chem. 21 (2015) 405-413.

Figure legends:

Fig. 1 (a) Time-resolved UV-vis spectra of $AgNO_3$ reaction solutions, (b) Change in absorption at 420 nm at different reaction times. The inset shows digital photographs of the AgNPs solution, (c) Effect of storage (in months) on the UV-vis spectra of AgNPs in the reaction solution (corresponding digital photographs are shown in the inset), (d) Effect of storage (in months) on the UV-vis spectra of ultracentrifuged AgNPs (corresponding digital photographs are shown in the inset).

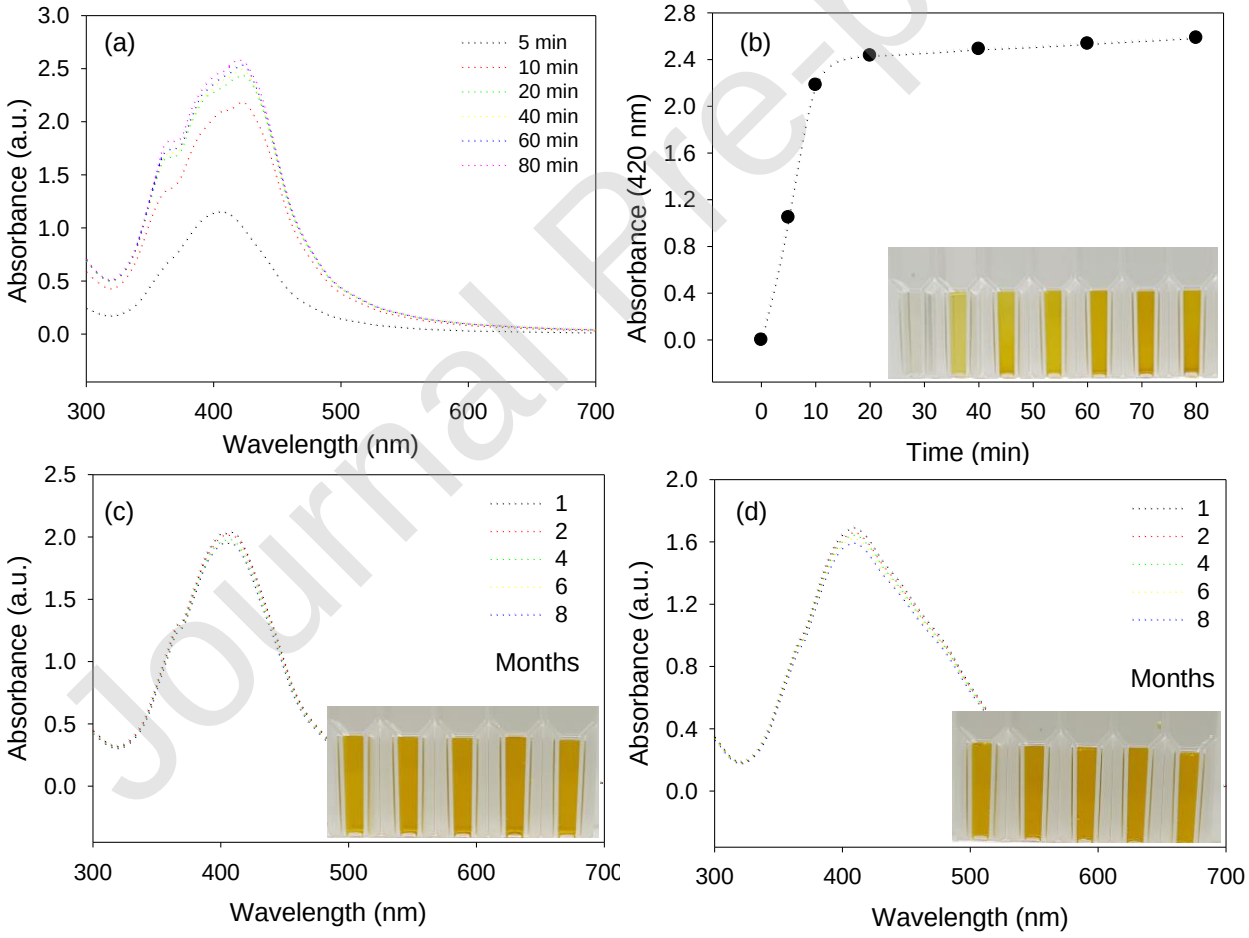

Fig. 2 (a) XPS survey spectra of the AgNPs, (b) high-resolution Ag3d spectra of the AgNPs, (c) XRD spectra of the AgNPs, (d) TEM image of the AgNPs.

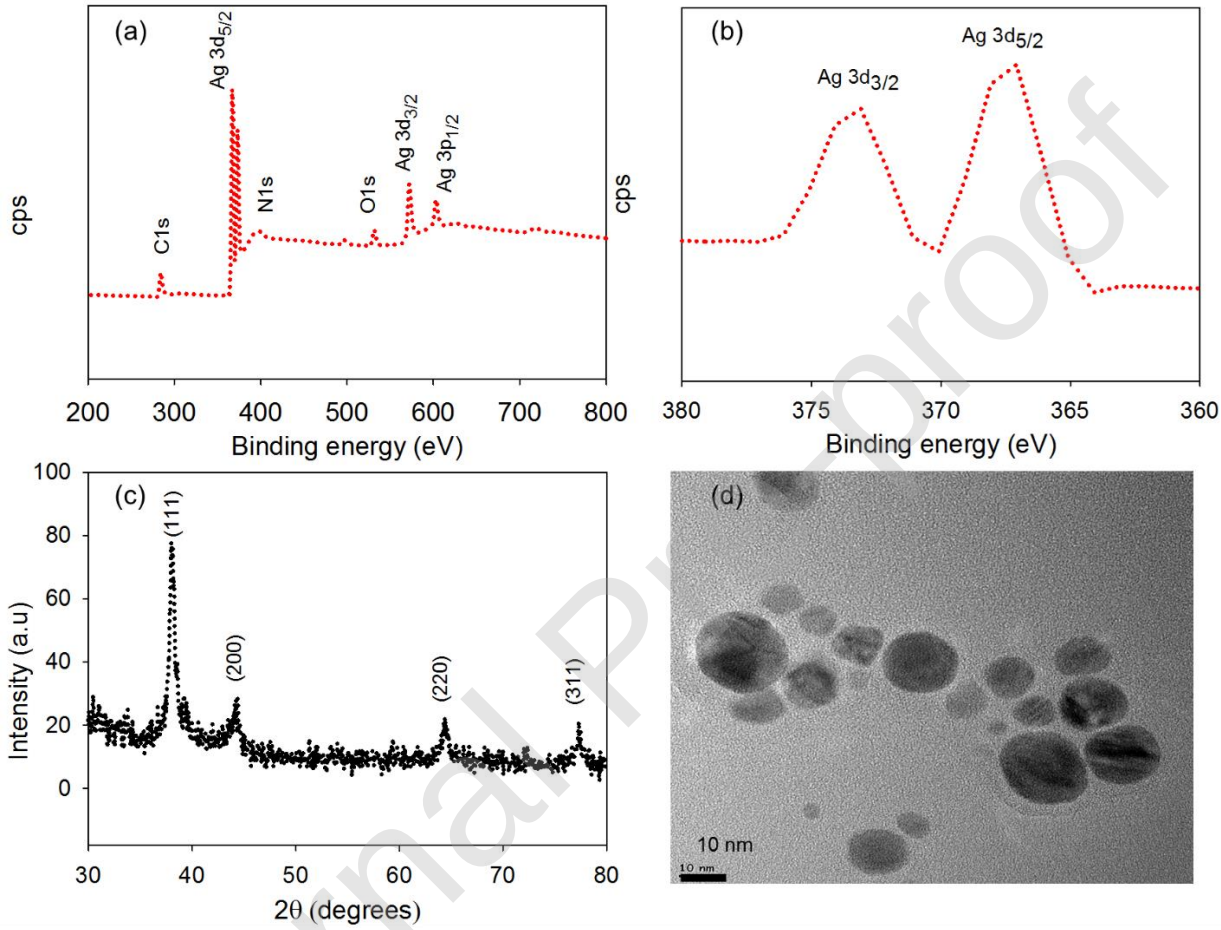

Fig. 3 (a,b) UV-vis absorption spectra of the AgNPs upon the addition of different metals, (c,d) Corresponding absorbance intensity recorded at 525 nm for various metallic ions. The inset shows the colorimetric changes of the AgNPs in the presence of various metal ions.

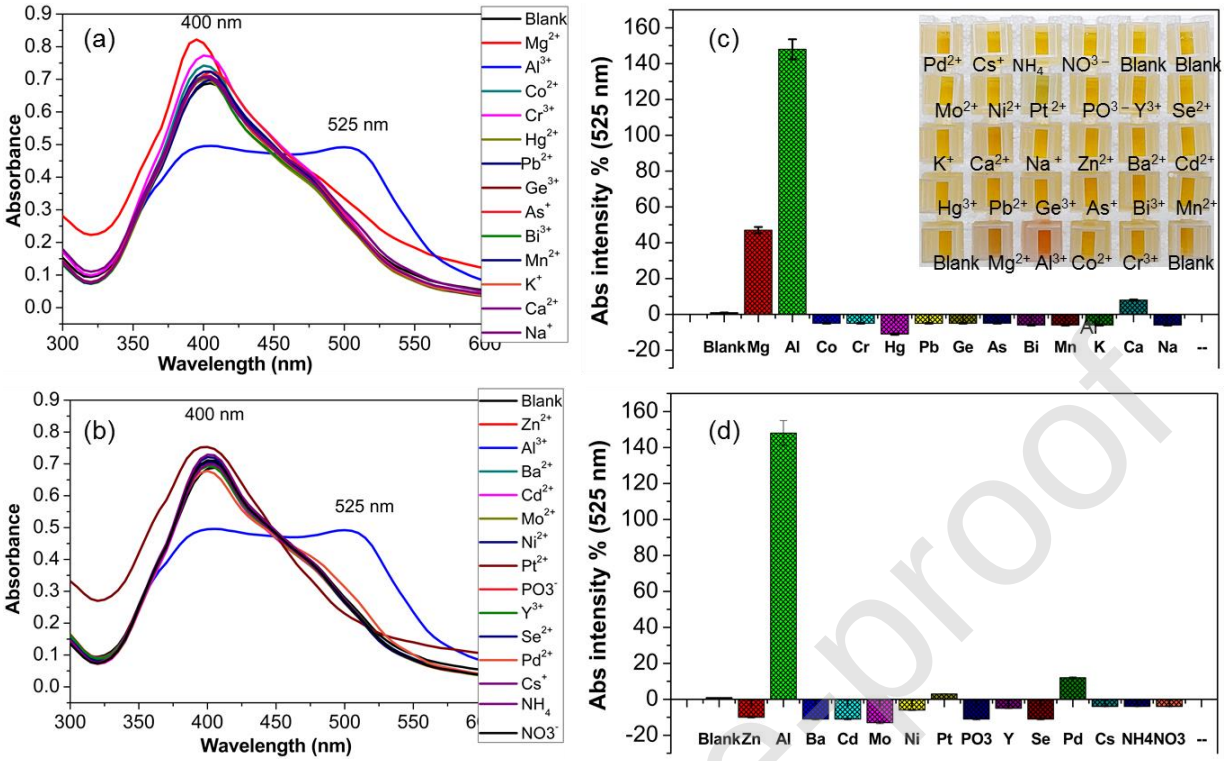

Fig. 4 (a) Absorption spectra and color of the AgNP solutions after addition of a narrow concentration range of Al^{3+} from 0.37 to 2.22 µM, (b) Plot of absorbance intensity recorded at 400 nm for the narrow concentration range of Al^{3+} from 0.37 to 2.22 µM, (c) Plot of absorbance intensity recorded at 525 nm for the narrow concentration range of Al^{3+} from 0.37 to 2.22 µM, (d) Absorption spectra and color of the AgNP solutions after addition of a broad concentration range of Al^{3+} from 0.37 to 8.89 µM, (e) Plot of absorbance intensity recorded at 400 nm for the broad concentration range of Al^{3+} from 0.37 to 8.89 µM, (f) Plot of absorbance intensity recorded at 525 nm for the broad concentration range of Al^{3+} from 0.37 to 8.89 µM.

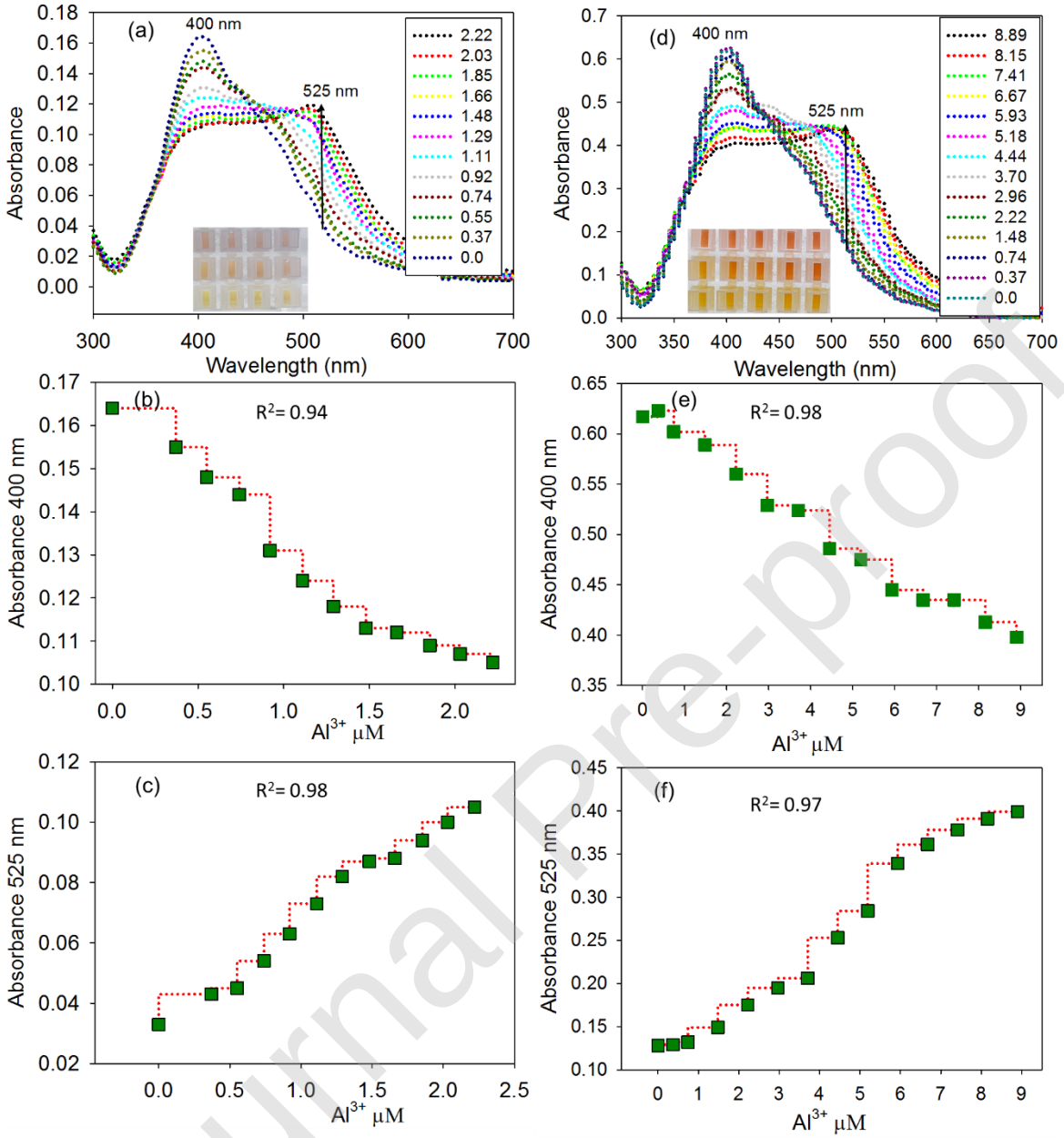

Fig. 5 (a) Absorbance intensity of our nanosensor probe in the presence of Al^{3+} at different pH, (b) Real-time (1 to 10 min) absorbance response of the AgNPs in the presence of Al^{3+} (4.44 µM).

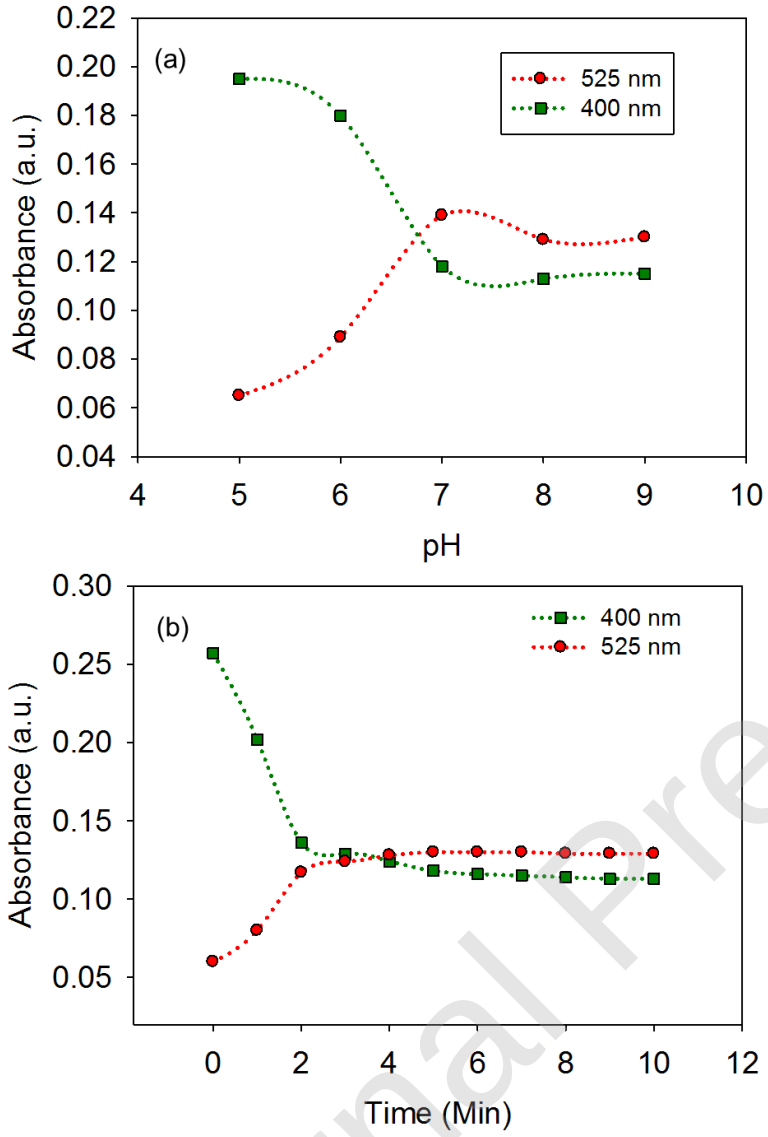

Fig. 6 (a) Decay profile of the absorbance response of the AgNPs recorded at 400 nm and increasing concentrations of Al^{3+}, as labeled in the graphs, (b) Decay profile of the absorbance response of the AgNPs recorded at 525 nm and increasing concentrations of Al^{3+}, as labeled in the graphs.

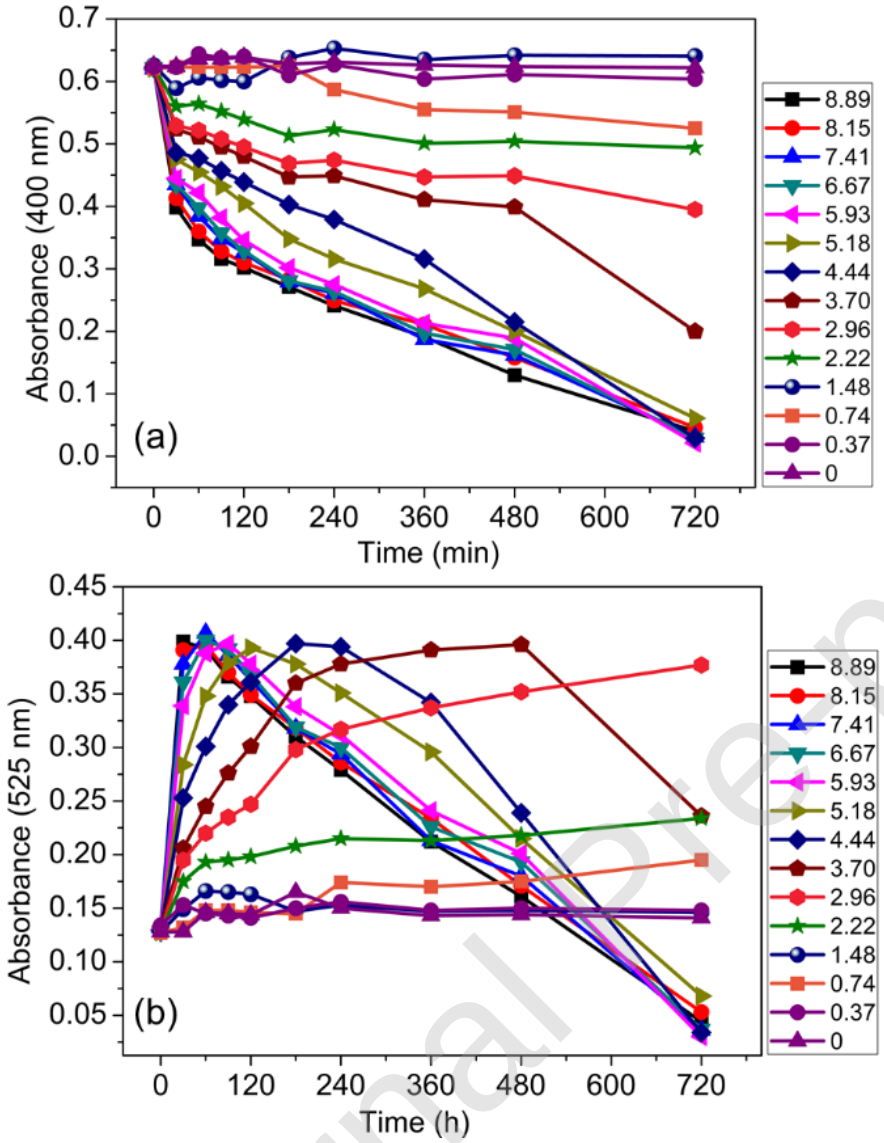

Fig. 7 TEM images of the AgNP solution in the absence (left) and presence of Al^{3+} (right). The inset shows images of the corresponding solutions.

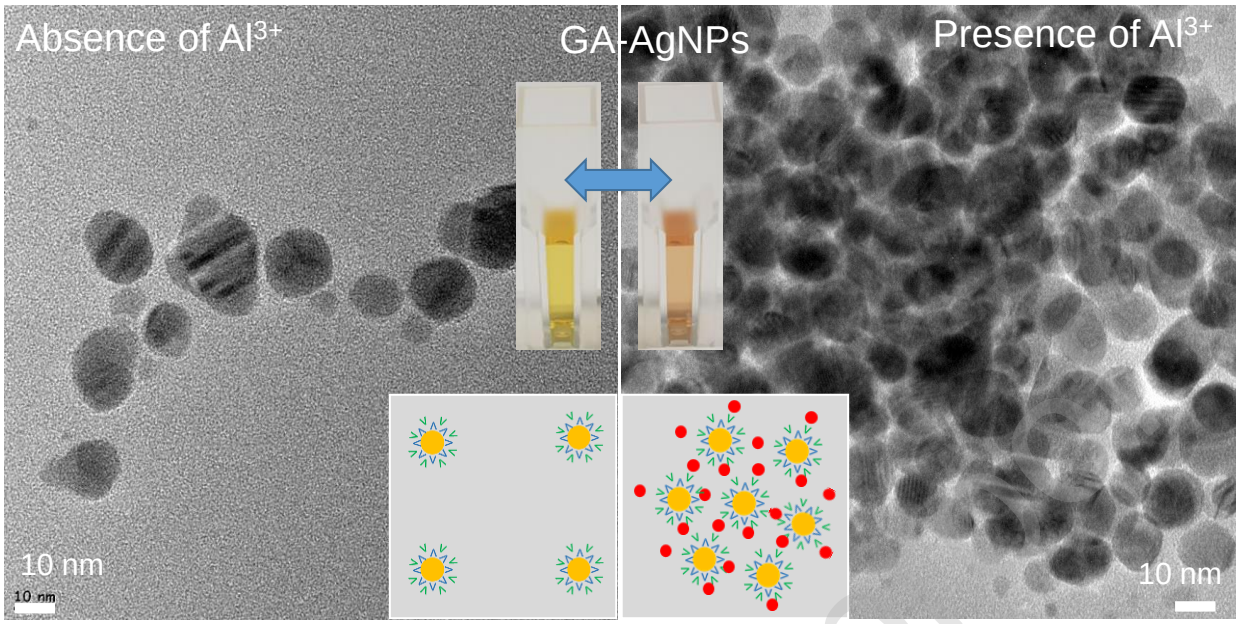

Fig. 8 (a) STEM imaging of the AgNP aggregates, (b) EDS of the AgNP aggregates in the presence of Al^{3+}, (c) Selected area of AgNP aggregates in the presence of Al^{3+}, (d) Reference image of selected AgNP aggregates in the presence of Al^{3+}, (e) Al elemental mapping of the AgNP aggregates, (f) Ag elemental mapping of the AgNP aggregates.

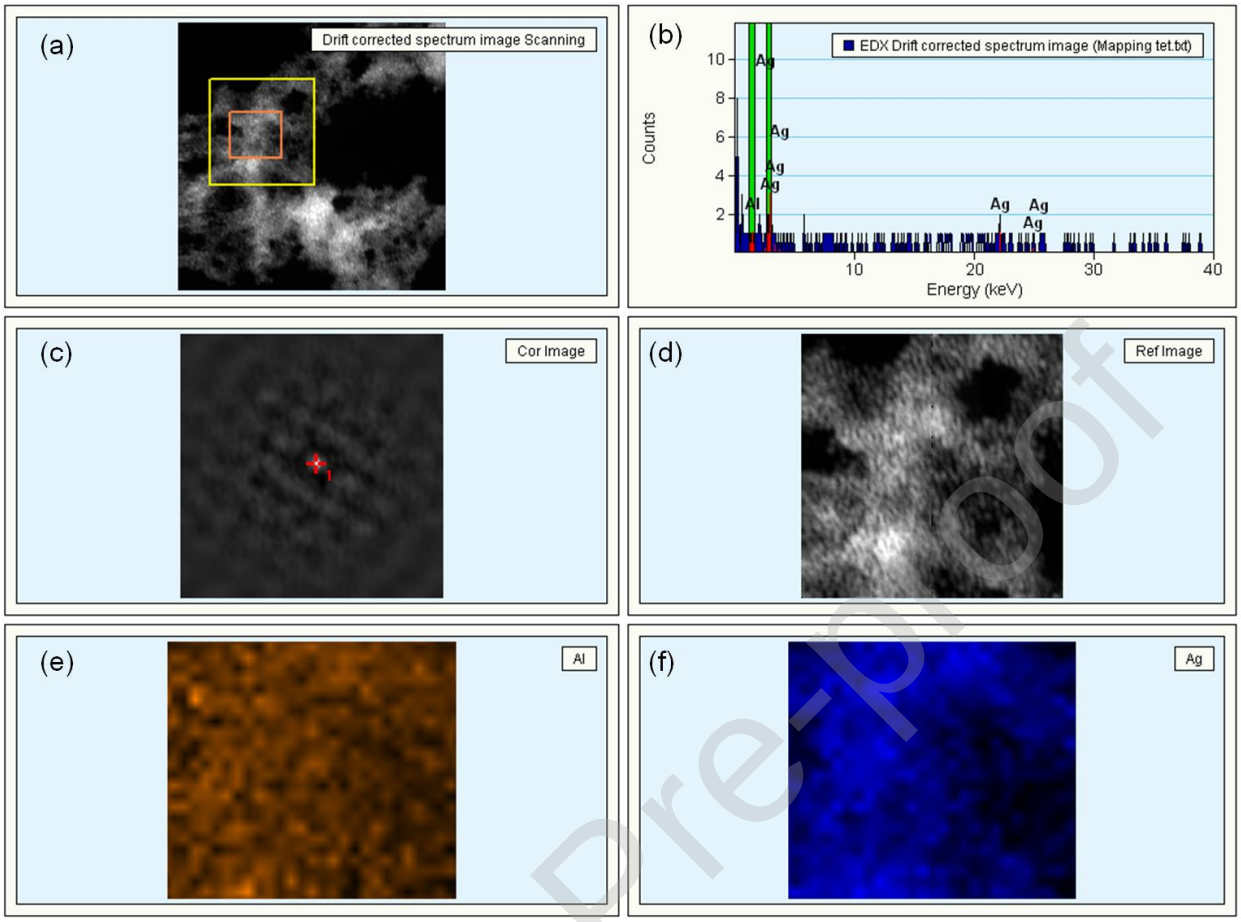

Supplementory materials:

Gallic acid-functionalized silver nanoparticles as colorimetric and spectrophotometric probe for detection of Al^{3+} in aqueous medium

Gajanan Ghodake[1], Surendra Shinde[1], Avinash Kadam[2], Rijuta Ganesh Saratale[2], Ganesh Dattatraya Saratale[3], Asad Syed[4], Omar H.M. Shair[4], Marzouq H. Alsaedi[4], and Dae-Young Kim[1*]

[1] Department Biological and Environmental Science, College of Life Science and Biotechnology, Dongguk University-Seoul, Ilsandong-gu, 10326, Goyang-si, Gyeonggi-do, Republic of Korea

[2] Research Institute of Biotechnology and Medical Converged Science, Dongguk University-Seoul, Ilsandong-gu, Goyang-si, Gyeonggi-do, 10326, Republic of Korea

[3] Department of Food Science and Biotechnology, Dongguk University-Seoul, Ilsandong-gu, Goyang-si, Gyeonggi-do, 10326, Republic of Korea

[4] Department of Botany and Microbiology, College of Science, King Saud University, P.O. 2455, Riyadh 11451, Saudi Arabia

Corresponding author:

Dae-Young Kim, PhD

Tel: +82-31-961-5122

Fax: +82-31-961-5122

Email: sbpkim@dongguk.edu

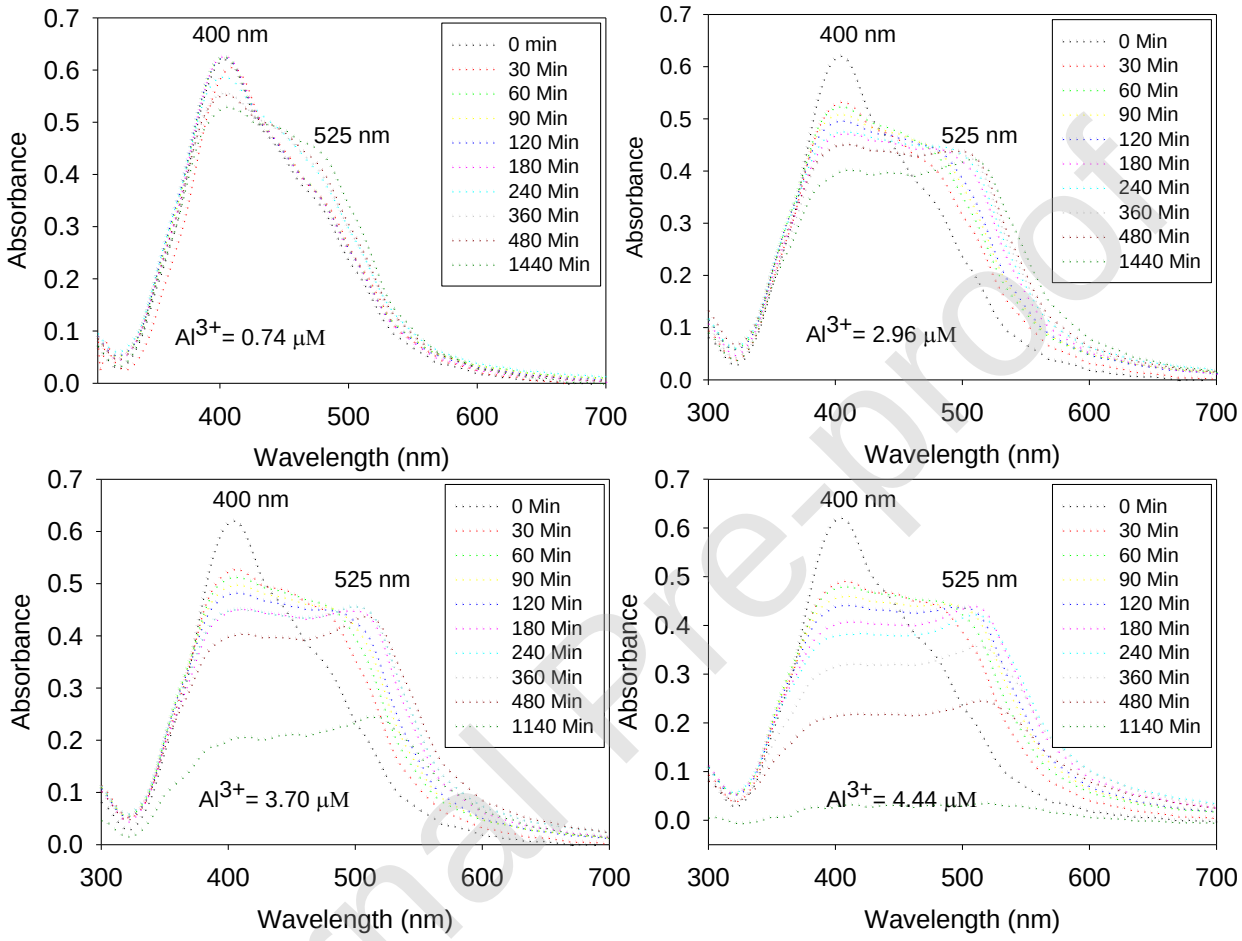

Fig. S1 Time course of the UV-vis spectra in the presence of four different concentrations of Al^{3+} as labeled in the figures.

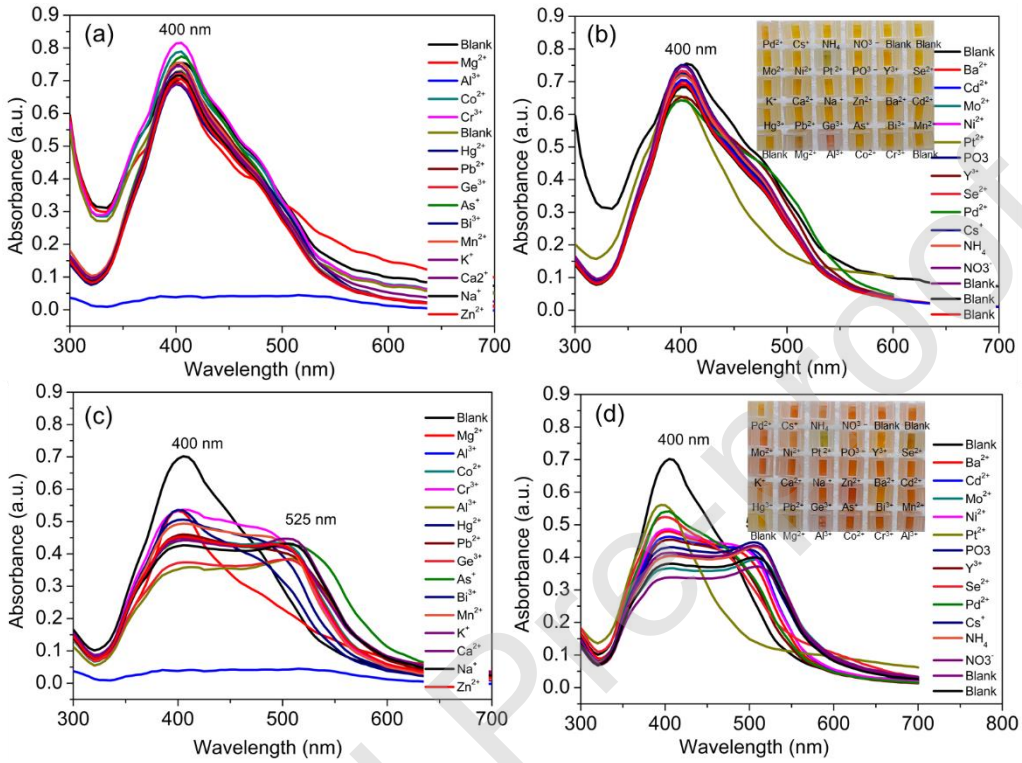

Fig. S2 (a) The effect of various metal ions on the UV-vis spectrum of GA-AgNPs over a 24 h incubation at ambient temperature, (b) The effect of various metal ions on the UV-vis spectrum of GA-AgNPs over a 24 h incubation at ambient temperature, (c) A wide range of metal ions did not exhibit significant interference on the detection of Al^{3+}, with the exception of Mg^{2+}, (d) A wide range of metal ions did not exhibit significant interference on the detection of Al^{3+}, with the exception of Pt^{2+}.

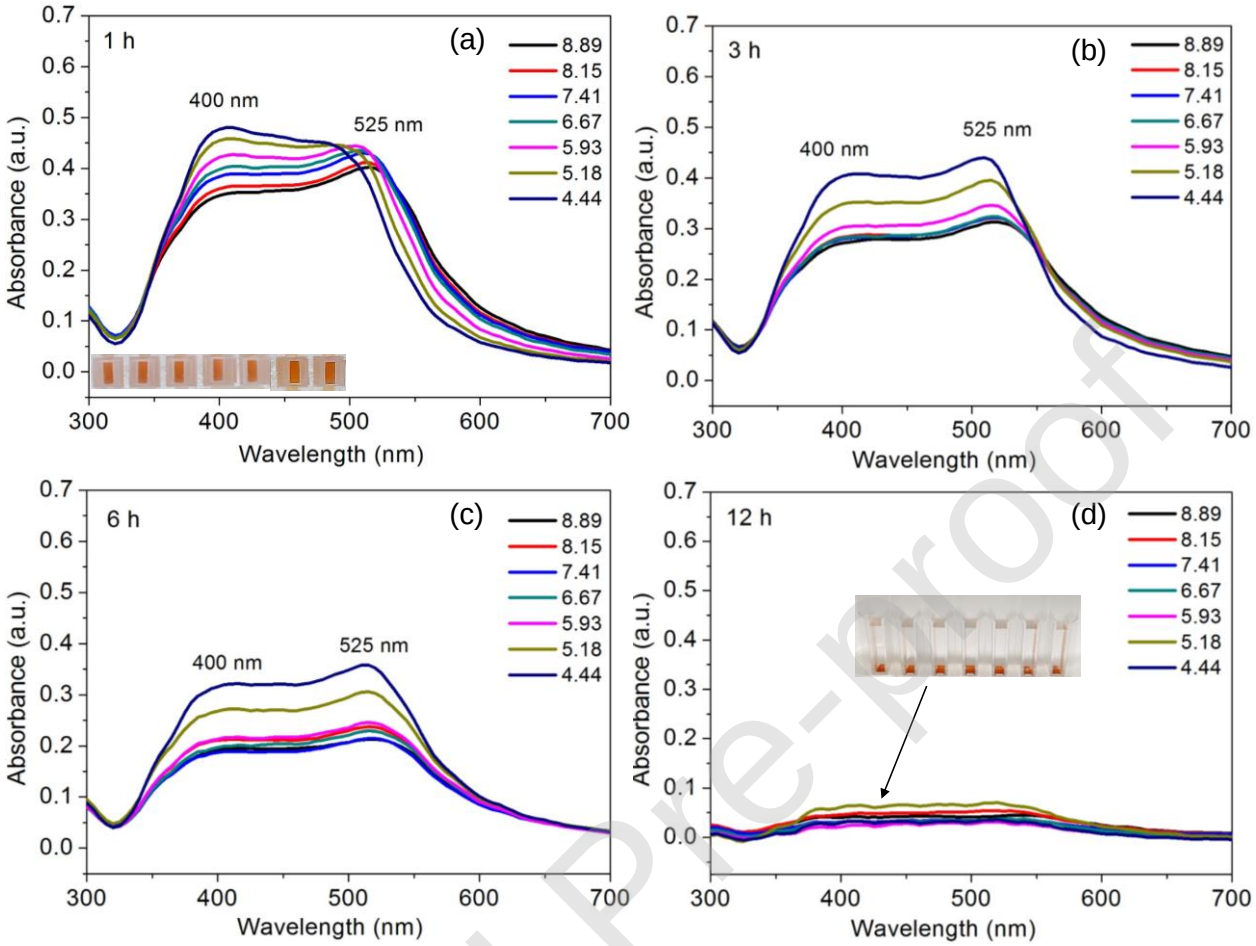

Fig. S3 Aggregation and sedimentation used for removal Al^{3+}-bound GA-AgNP probes (a) spectral profile of the AgNPs after a 1 h treatment with Al^{3+} (4.44 to 8.89 µM). The inset shows the color of the solutions after the Al^{3+} was mixed with the solution, (b) spectral profile of the AgNPs after a 3 h treatment with Al^{3+} (4.44 to 8.89 µM), (c) spectral profile of the AgNPs after a 6 h treatment with Al^{3+} (4.44 to 8.89 µM), (d) spectral profile of the AgNPs after a 12 h treatment with Al^{3+} (4.44 to 8.89 µM). The inset shows the sedimentation of the solutions after the Al^{3+} was mixed into the solution.

References

[1] J.C. Wesdock, I.M.F. Arnold, J. Occup. Environ. Med. 56 (2014) S5-S11.

[2] C. Exley, Environ. Sci. Process. Impacts 15 (2013) 1807.

[3] A.D. Semwal, A. Padmashree, M.A. Khan, G.K. Sharma, A.S. Bawa, J. Sci. Food Agric. 86 (2006) 2425.

[4] L.A. Al Juhaiman, J. Saudi Chem.Soc. 14 (2010) 131.

[5] J. Zhang, Z. Lyu, S. Shao, F. Li, S. Yang, W. Song, W. Li, S. Li, Chin. Geogr. Sci. 26 (2016) 495.

[6] S.J. Zheng, Ann. Bot. 106 (2010) 183.

[7] M. Kawahara, M. Kato-Negishi, J. Alzheimers Dis. 2011 (2011) 276393.

[8] S.C. Bondy, NeuroToxicol. 52 (2016) 222.

[9] J.-B. Liu, W. Wang, G. Li, R.-X. Wang, C.-H. Leung, D.-L. Ma, ACS Omega 2 (2017) 9150.

[10] T. Han, X. Feng, B. Tong, J. Shi, L. Chen, J. Zhi, Y. Dong, Chem. Comm. 48 (2012) 416.

[11] A. Sanz-Medel, A.B. Soldado Cabezuelo, R. Milačič, T. Bantan Polak, Coord. Chem. Rev. 228 (2002) 373.

[12] M.H. Mashhadizadeh, M. Amoli-Diva, J. Anal. Atom. Spectrom. 28 (2013) 251.

[13] M. Frankowski, A. Zioła-Frankowska, I. Kurzyca, K. Novotný, T. Vaculovič, V. Kanický, M. Siepak, J. Siepak, Environ. Monit. Assess. 182 (2011) 71.

[14] A.M. Asiri, M.M. Hussain, M.N. Arshad, M.M. Rahman, J. Ind. Eng.Chem. 63 (2018) 312.

[15] S.M. Hossain, A. Lakma, R.N. Pradhan, A. Chakraborty, A. Biswas, A.K. Singh, RSC Adv. 5 (2015) 63338.

[16] S.H. Kim, H.S. Choi, J. Kim, S.J. Lee, D.T. Quang, J.S. Kim, Org. Lett. 12 (2010) 560.

[17] W. Lin, L. Yuan, J. Feng, Eur. J. Org. Chem. 2008 (2008) 3821.

[18] E.M.S. Azzam, A.F.M. El-farargy, A.A. Abd-Elaal, J. Ind. Eng. Chem. 20 (2014) 3905.

[19] U. Jeong, Y. Kim, J. Ind. Eng. Chem. 31 (2015) 393.

[20] K. Singh, D. Kukkar, R. Singh, P. Kukkar, K.-H. Kim, J. Ind. Eng. Chem. (2018).

[21] Y. Mizukami, Y. Sawai, Y. Yamaguchi, J. Agri. Food Chem. 55 (2007) 4957.

[22] M.n. Ó'Coinceanainn, M.J. Hynes, J. Inorg. Biochem. 84 (2001) 1.

[23] D.-Y. Kim, M. Kim, S. Shinde, J.-S. Sung, G. Ghodake, Colloids Surf. B Biointerfaces, 149 (2017) 162.

[24] D. Li, Z. Liu, Y. Yuan, Y. Liu, F. Niu, Pro. Biochem.50 (2015) 357-366.

[25] D.-Y. Kim, J. Suk Sung, M. Kim, G. Ghodake, Mater. Lett. 155 (2015) 62.

[26] J. Polte, Cryst. Eng. Comm. 17 (2015) 6809.

[27] D.-S. Park, H. Wang, S.K. Vasheghani Farahani, M. Walker, A. Bhatnagar, D. Seghier, C.-J. Choi, J.-H. Kang, C.F. McConville, Sci. Rep. 6 (2016) 18449.

[28] J.I. Hussain, A. Talib, S. Kumar, S.A. Al-Thabaiti, A.A. Hashmi, Z. Khan, Colloids Surf. A Physicochem. Eng. Asp. 381 (2011) 23.

[29] C.-N. Lok, C.-M. Ho, R. Chen, Q.-Y. He, W.-Y. Yu, H. Sun, P.K.-H. Tam, J.-F. Chiu, C.-M. Che, J. Biol. Inorg. Chem. 12 (2007) 527.

[30] T.L. Moore, L. Rodriguez-Lorenzo, V. Hirsch, S. Balog, D. Urban, C. Jud, B. Rothen-Rutishauser, M. Lattuada, A. Petri-Fink, Chem. Soc. Rev. 44 (2015) 6287.

[31] J.D. Robertson, L. Rizzello, M. Avila-Olias, J. Gaitzsch, C. Contini, M.S. Magoń, S.A. Renshaw, G. Battaglia, Sci. Rep. 6 (2016) 27494.

[32] I.E. dell'Erba, C.E. Hoppe, R.J.J. Williams, Langmuir, 26 (2010) 2042-2049.

[33] R. Azadbakht, J. Khanabadi, Tetrahedron 69 (2013) 3206.

[34] H. Lee, H.K. Sung, C. Park, Y. Kim, J. Ind. Eng. Chem. 48 (2017) 235-241.

[35] Y. Chen, T. Wei, Z. Zhang, T. Chen, J. Li, J. Qiang, J. Lv, F. Wang, X. Chen, Ind. Eng. Chem. Res. 56 (2017) 12267.

[36] W. Cao, X.-J. Zheng, J.-P. Sun, W.-T. Wong, D.-C. Fang, J.-X. Zhang, L.-P. Jin, Inorg. Chem. 53 (2014) 3012.

[37] A. Kumar, M. Bhatt, G. Vyas, S. Bhatt, P. Paul, ACS Appl. Mater. Interfaces 9 (2017) 17359.

[38] A.L. Suherman, E.E.L. Tanner, S. Kuss, S.V. Sokolov, J. Holter, N.P. Young, R.G. Compton, Sens. Actuators B Chem. 265 (2018) 682.

[39] P. Joshi, R. Painuli, D. Kumar, ACS Sustain. Chem. Eng. 5 (2017) 4552.

[40] L. Zhang, R. Liu, B.W. Gung, S. Tindall, J.M. Gonzalez, J.J. Halvorson, A.E. Hagerman, J. Agri. Food Chem. 64 (2016) 3025.

[41] Z. Liu, Y. Li, Y. Ding, Z. Yang, B. Wang, Y. Li, T. Li, W. Luo, W. Zhu, J. Xie, C. Wang, Sens. Actuators B: Chem. 197 (2014) 200.

[42] M. Shyamal, P. Mazumdar, S. Maity, G.P. Sahoo, G. Salgado-Morán, A. Misra, J. Phy. Chem. A 120 (2016) 210.

[43] A.K. Saini, V. Sharma, P. Mathur, M.M. Shaikh, Sci. Rep. 6 (2016) 34807.

[44] N. Yang, Y. Gao, Y. Zhang, Z. Shen, A. Wu, Talanta 122 (2014) 272.

[45] T. Okuda, W. Nishijima, M. Sugimoto, N. Saka, S. Nakai, K. Tanabe, J. Ito, K. Takenaka, M. Okada, Water Res. 60 (2014) 75.

[46] D.R.C. McLachlan, C. Bergeron, P.N. Alexandrov, W.J. Walsh, A.I. Pogue, M.E. Percy, T.P.A. Kruck, Z. Fang, N.M. Sharfman, V. Jaber, Y. Zhao, W. Li, W.J. Lukiw, Mol. Neurobiol. (2019).

[47] S. Chen, Y.-M. Fang, Q. Xiao, J. Li, S.-B. Li, H.-J. Chen, J.-J. Sun, H.-H. Yang, Analyst 137 (2012) 2021.

[48] D.-Y. Kim, S. Shinde, G. Ghodake, J Colloid Interf. Sci. 494 (2017) 1.

[49] M. Abdel Salam, G. Al-Zhrani, S.A. Kosa, J. Ind. Eng. Chem. 20 (2014) 572.

[50] V. Rondeau, D. Commenges, H. Jacqmin-Gadda, J.F. Dartigues, Am. J. Eepidemiol. 152 (2000) 59.

[51] M. Ghaedi, M. Montazerozohori, N. Rahimi, M.N. Biysreh, J. Ind. Eng. Chem. 19 (2013) 1477-1482.

[52] R. Asrarian, R. Jadidian, H. Parham, S. Haghtalab, Adv. Mater. Res. 829 (2014) 752.

[53] R. Zhu, J. Song, Q. Ma, Y. Zhou, J. Yang, S. Shuang, C. Dong, Anal. Meth. 8 (2016) 7232.

[54] M.R. Awual, M.A. Khaleque, Y. Ratna, H. Znad, J. Ind. Engi.Chem. 21 (2015) 405-413.

[55] H. Peng-Cheng, F. Hao, X. Jing-Jing, W. Fang-Ying, Meth. Appl. Fluor. 5 (2017) 024014.

[56] V.K. Gupta, S.K. Shoora, L.K. Kumawat, A.K. Jain, Sens. Actuators B: Chem. 209 (2015) 15.

Table. 1. Detection of Al^{3+} content based on different methods and approaches.

Method	Chemistry	LOD	Reference
Fluorescent	Benzothiazole	2.2 µM	[35]
Fluorescent	Chemosensor	3.3 µM	[36]
Fluorescent	Schiff-base	1.98 µM	[55]
Colorimetric	Polyacrylate	2.0 µM	[37]
Colorimetric	Chemosensor	1.81 µM	[56]
Colorimetric	Gallic acid	0.55 µM	This work

Table. 2. Determination of the concentration of spiked Al^{3+} using the present method and comparisons with ICP-MS. *ND = not detected.

Sr. No.	Water samples	Spiked Al^{3+} (µM)	ICP-MS results (µM)	Colorimetric results (µM)
1	Lake water	0.0 2.0	ND 2.18	ND 2.24 ±0.037
	River water	0.0 3.7	ND 3.84	ND 3.96 ±0.051
3	Wastewater	0.0 4.44	0.68 5.29	0.76 ±0.013 5.37 ±0.072
4	Tap water	0.0 5.18	ND 5.32	ND 5.43 ±0.078
5	DI water	0.0 7.40	ND 7.51	ND 7.62 ±0.089